A Theoretical Insight into the Photophysics of Acridine

Òscar Rubio-Pons, Luis Serrano-Andrés,* and Manuela Merchán

Departamento de Química Física, Instituto de Ciencia Molecular, Universitat de València, Dr. Moliner 50, Burjassot, E-46100, Valencia, Spain

Received: August 10, 2001

The electronic absorption and emission spectra of acridine have been studied by means of a multiconfigurational second-order perturbation method (CASSCF/CASPT2) and its multistate extension (MS-CASPT2). The low-lying valence singlet and triplet $\pi \rightarrow \pi^*$ and $n \rightarrow \pi^*$ excited states have been computed. The location of the lowest Rydberg state (3s) has been also estimated. By optimization of the geometries of the ground and low-lying excited states and the calculation of transition energies and properties, the obtained results lead to a complete analysis and assignment of the available experimental singlet−singlet and triplet−triplet absorption spectra and to the description of the basic features of the fluorescence and phosphorescence processes of acridine. The photophysics of acridine and its protonated form are analyzed and the effects of solvation are discussed. The present findings support the model of a state reversal on the lowest singlet excited state upon increasing the solvent polarity.

1. Introduction

Acridine is an important aza-aromatic compound mainly used as a staining dye for biological tissues. Its derivatives have significant antibacterial and potential antiviral activity and have been widely used in pharmacology.[1,2] Due to their prominent chelating properties, acridines also have been used as ligands for heavy metals in different areas of chemistry.[3] As regards the photochemistry of these compounds, the attention has been mainly focused on the chemiluminiscence of acridine, a process with a high quantum yield similar to those occurring in luminol and lucigenin.[4,5] Two main questions in the photophysics of acridine have been put forward: first, the solvent dependence of the observed fluorescence; second, the build up of triplet states.[6−9] There are, however, many other aspects to be solved, such as the nature and character of the lowest singlet and triplet excited states, a controversy constantly found in the experimental literature,[10−14] and the understanding of the triplet−triplet absorption manifold, in which the most intense feature has not been yet characterized.[7−9,12,15] Previous theoretical studies performed with semiempirical methods[16−18] could not answer, however, many of these questions. The present CASSCF/MS-CASPT2 study aims to a detailed and accurate study of the geometries, excitation energies, and transition properties involving the low-lying $\pi \rightarrow \pi^*$ and $n \rightarrow \pi^*$ excited states of the acridine molecule in order to get insight into the rich photophysics of the system, both in absorption and emission.

Two main bands form the measured absorption spectrum of acridine.[2,19,20] A low-lying and structured band is observed near the visible region, starting at 3.2 eV and peaking at 3.5 eV[7,10−12,19−21] being considered as a mixture of the ^1L_b and ^1L_a $\pi \rightarrow \pi^*$ states of Platt's nomenclature,[22] long and short-axis polarized, respectively.[13,20] The lowest $n \rightarrow \pi^*$ excited state has been proposed to lie in the same energy region, although the detection of the state has been problematic[13] because of the overlap with the $\pi \rightarrow \pi^*$ features. The influence of the environment, temperature, and protonation on the band shape and position have been extensively studied.[11] In acidic water solutions the maxima of the absorption band remains basically unaltered and a broad shoulder centered around 3.10 eV can be observed.[7,11] A second and more intense band in the acridine absorption spectrum is located peaking near 5.0 eV.[2,19,20] As shown below, it has a complex structure and it is composed of several $\pi \rightarrow \pi^*$ and $n \rightarrow \pi^*$ electronic transitions. In a less studied energy region of the spectrum, a broad band centered at 5.9 eV[2,20] is clearly observed in different solvents.

As regards the emission spectroscopy of acridine, most of the studies have been devoted to the description of the relative position of the low-lying singlet and triplet states and the definition of the photophysical paths and their dependence on the environmental conditions.[6,7,23] The intense fluorescence reported in protic solvents with large lifetimes has been attributed to the presence of a $\pi \rightarrow \pi^*$ state as the lowest singlet state in polar environments. On the other hand, the low fluorescence quantum yield in the vapor and nonpolar solvents,[6,8,9] has been explained by a more stable $n \rightarrow \pi^*$ state and the predominance of nonradiative processes such as intersystem crossings and internal conversions in these media. The influence of the state reversal and the effect of the vibronic coupling (the so-called proximity effect[24,25]) on the final photophysics of acridine is a controversial issue of current interest.[2,10,23,26] The effects of temperature, protonation, and gas or crystal matrices on the fluorescence process have also been studied[7,11,12,23,27,28] and will be discussed below. The triplet−triplet spectra of acridine in different solvents and the study of the formation rate of the lowest triplet state[7−9] have been reported as indirect ways to determine the radiationless mechanisms in the corresponding emission spectra. A clear assignment of the two bands of the absorption triplet−triplet spectra has not been yet achieved. Moreover, their controversial behavior found in different solvents[7−9] requires further analysis.

The present contribution aims to obtain reliable data to characterize the electronic states of acridine and their transition properties, both in absorption and emission, and give an accurate account of the static aspects of the photophysics of the isolated

* Author for correspondence: Luis.Serrano@uv.es

10.1021/jp013124m CCC: $20.00
Published on Web 10/03/2001

molecule, in order to get insight into some of the many phenomena related with the spectroscopy of the system. The CASSCF/MS-CASPT2 method[29−32] has proved to be an accurate tool to determine electronic state and transition properties. Geometry optimizations of the ground and low-lying singlet and triplet valence states have been performed at the CASSCF level of calculation. The absorption spectrum of acridine up to 6.0 eV has been studied at the ground-state geometry, while absorption and emission band origins and maxima have been obtained at the respective optimized geometry of the excited states. The position of the lowest Rydberg transition has also been calculated. Dipole moments of the excited states, as well as oscillator strengths, transition rates, and radiative lifetimes will be computed and used to assign, discuss, and clarify different aspects of the spectroscopy of acridine. Finally, selected calculations will be performed on the protonated acridinium ion to get more information on the effects of protonation in the low-lying excited states of the system.

2. Methods and Computational Details

Geometries for the ground and excited states were optimized by computing analytical CASSCF gradients. An active space of 12 active electrons (10 π, 2 lone-pair n) in 13 molecular orbitals (12 π, 1 n) was used in all the calculations except when indicated. The lowest orbital of each of the π symmetries (b_1 and a_2) was kept inactive. The molecule is placed on the zy plane with z as the C_2 axis containing the nitrogen atom. The C_{2v} symmetry is maintained all the time. The employed active space can be therefore labeled (1705) within the symmetries ($a_1b_1b_2a_2$). The choice of the active space has been guided by the experience in precedent works for similar systems such as naphthalene, indole analogues, stilbene, etc.[33,34] and by checking carefully the convergence of the employed methods for the number of excited states included in the study.

An ANO type basis set[35] contracted to C, N[4s3p1d]/H [2s1p] was used in all the cases except for the calculation of the 3s Rydberg state. This basis has proved its accuracy in many previous situations.[31,32,36] For the calculation of the lowest Rydberg state, an additional s diffuse function was added to the previous valence basis set at the charge centroid of the acridine cation. The coefficients of the diffuse basis were optimized for the cation following a procedure described elsewhere.[36] This specific calculation on the 3s Rydberg state included one additional a_1 active orbital in order to take the Rydberg orbital into account, giving rise to an active space (2705). In the calculations of the vertical excitation energies, the carbon and nitrogen 1s core electrons were kept frozen in the form of the ground-state SCF wave function.

In the vertical calculations at the respective geometries, the CASSCF wave functions are generated as state-average (SA) CASSCF roots within a given symmetry. The number of roots has been chosen in order to contain all the important states at low energies. In the vertical calculations at the ground-state geometry, nine, eight, four, and three roots of the $^1A_1$, $^1B_2$, $^1B_1$, and $^1A_2$ symmetries were used, respectively. The calculations on the triplet states included five roots, both at the singlet ground state and lowest triplet state geometries. Finally, at each of the excited-state geometries, three roots were included in the treatment for all the symmetries. Using these multiconfigurational functions as reference, second-order perturbation theory is employed to include the dynamical correlation energy effects, the CASPT2 method,[29,37] where each root is computed independently. To prevent the undesirable influence of intruder states, the level-shift (LS) technique was employed.[38] The presence of spurious influences in the wave function is enhanced by the use of enlarged and diffuse functions such as those of the ANO-type basis sets. The parameter employed to apply the LS method is always selected after studying the stability of the energy and the weight of the reference wave function. Here a parameter of 0.3 au was employed in all cases.

Finally, an extension of the CASPT2 calculations, the multistate (MS) CASPT2 method,[30] was used. In general, the MS-CASPT2 approach can be useful when CASPT2 cannot account for the mixing of states in cases where the CASSCF wave function is not a good reference and a strong mixing occurs between the reference state and one or more additional CAS-CI states, for instance when crossing of states or strong valence-Rydberg mixing takes place. The MS-CASPT2 method uses a multidimensional reference space that is spanned by the SA-CASSCF roots, leading to the interaction of these states. The linear combination of the CAS states produced by the MS-CASPT2 computation has been named perturbatively modified CAS (PMCAS) CI wave function.[30] The PMCAS-CI wave function will be finally used to compute transition and state properties. The present calculations are one of the many situations where the addition of the MS-CASPT2 results to the CASPT2 energies will be of minor importance because the interaction of the CASPT2 states is weak. The MS-CASPT2 approach, however, is especially sensitive to the good convergence of the CASSCF wave function and to the absence of intruder states. In other words, the weight of the reference function for the computed excited states must be very close to the weight of the reference function for the ground state (closer than it has been acceptable for the CASPT2 method in past studies[38]), otherwise the interaction among the CASPT2 roots will be artificially large. For this reason, the final calculations on the $^1A_1$ and $^1B_2$ states used an active space (0805) in order to prevent intruder state interactions that, although affected the excitation energies in a minor extent, had large effects in the PMCAS-CI properties. The $^1A_1$ and $^1B_2$ excited states of the protonated acridinium ion were also computed at the same level of theory employing the MP2/6-31G* optimized ground-state geometry and the active space (0705).

The CASSCF state interaction (CASSI) method[39,40] was used to obtain the transition properties. The oscillator strengths were computed using PMCAS-CI transition dipole moments and MS-CASPT2 excitation energies. In the calculation of the spontaneous emission rates (Einstein's coefficients A_{21}) and radiative lifetimes (τ_{rad}), absorption transition dipole moments computed at the ground-state geometry and energy differences (E_{ve}, vertical emission) computed at the different excited states optimal geometries were used. In particular, the following expression was employed:

$$A_{21} = \frac{1}{\tau_{rad}} = 2.142005 \times 10^{10} < \psi_1|\mu|\psi_2 >^2 E_{ve}^3$$

where A_{21} is measured in s^{-1}, τ_{rad} in s, the dipole moment operator μ in au, the energy difference E_{ve} in au, and ψ_1 and ψ_2 are the wave functions of the ground and excited states, respectively.[41]

All calculations were performed with the MOLCAS-5.0 quantum chemistry software.[42]

3. Results and Discussion

The next sections describe the obtained theoretical results, comparison with experimental data, and discussions about the photophysics of acridine in the context of the present findings.

TABLE 1: Optimized Geometries for the Ground and the Low-lying Valence Excited States of Acridine[a]

parameters[b]	1^1A_1	1^1B_1	2^1A_1	1^1B_2	1^3A_1	1^3B_1	1^3B_2
$R(C_1-C_2)$	1.358	1.392	1.478	1.385	1.420	1.386	1.423
$R(C_2-C_3)$	1.439	1.390	1.344	1.429	1.355	1.397	1.429
$R(C_3-C_4)$	1.341	1.401	1.444	1.358	1.418	1.393	1.343
$R(C_4-C_5)$	1.440	1.376	1.387	1.415	1.390	1.382	1.453
$R(C_5-C_6)$	1.421	1.424	1.438	1.474	1.437	1.420	1.437
$R(C_6-C_7)$	1.393	1.427	1.419	1.413	1.425	1.422	1.405
$R(C_6-C_1)$	1.436	1.403	1.384	1.410	1.387	1.409	1.409
$R(C_5-N)$	1.332	1.361	1.356	1.347	1.364	1.381	1.333
$R(C_1-H_1)$	1.075	1.075	1.076	1.075	1.075	1.075	1.074
$R(C_2-H_2)$	1.074	1.074	1.072	1.073	1.074	1.074	1.073
$R(C_3-H_3)$	1.074	1.076	1.076	1.074	1.074	1.074	1.074
$R(C_4-H_4)$	1.074	1.074	1.073	1.073	1.073	1.074	1.073
$R(C_7-H_7)$	1.076	1.074	1.075	1.074	1.074	1.074	1.075
$\angle(C_2C_1C_6)$	120.5	121.2	121.6	120.9	120.9	121.2	120.6
$\angle(C_2C_1H_1)$	120.7	120.1	119.5	120.2	119.6	120.1	119.8
$\angle(C_6C_1H_1)$	118.8	118.7	118.9	118.9	119.5	118.6	119.6
$\angle(C_2C_3C_4)$	120.8	120.5	122.1	121.0	120.1	120.3	120.7
$\angle(C_3C_4C_5)$	120.8	119.4	121.3	121.2	120.8	119.4	121.3
$\angle(C_4C_5C_6)$	118.8	121.6	116.6	118.5	119.2	121.8	119.0
$\angle(C_4C_5N)$	118.3	124.6	120.9	118.8	118.1	124.1	118.1
$\angle(C_6C_7H_7)$	120.2	118.9	120.0	120.2	120.1	119.1	120.1

[a] CASSCF(13,12)/ANO C,N [4s3p1d]/H [2s1p] level. Constrained to C_{2v} symmetry. [b] Bond lengths (R) in Ångtroms and angles ($\angle$) in degrees. See Figure 1 for atom labeling and orientation.

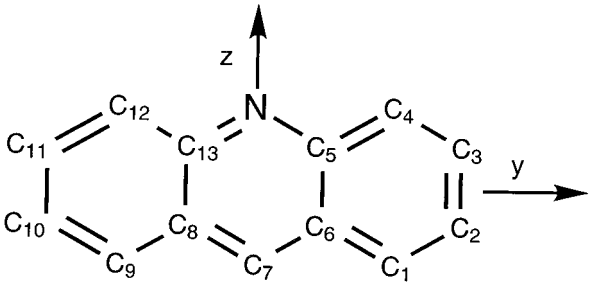

Figure 1. Atom labeling and molecular orientation used in acridine. The hydrogen atoms (not drawn) have the label of their respective carbon atom.

Section 3.1 describes the computed optimized geometries for the ground and low-lying excited states of the acridine molecule; section 3.2 deals with the vertical absorption spectrum of the system at the ground-state optimized geometry; section 3.3 describes the computed vertical triplet−triplet absorption spectrum of acridine at the geometry of the lowest triplet excited state; finally, section 3.4 reports on the emission spectra of acridine, and comments on the overall photophysics of the system in the vapor and in solvated media, including also the effects of protonation.

3.1 Geometries of the States. Table 1 compiles the optimized CASSCF geometries for several excited states of the acridine molecule. Figure 1 displays the acridine molecule and the labels of the atoms. In addition to the ground state, six low-lying $\pi \rightarrow \pi^*$ and $n \rightarrow \pi^*$ singlet and triplet excited states have been optimized in order to have all the necessary information to analyze the absorption and emission properties of the system. At the ground-state optimized geometry, the singlet−singlet and singlet−triplet vertical absorption spectra have been computed; at the optimized geometry for the lowest triplet state, the triplet−triplet vertical absorption spectrum has been analyzed, and, finally, at the corresponding optimized geometries of the different excited states, the vertical emission energies have been obtained. The combination of ground and excited states energies at their respective optimal geometries leads to the estimation of band origins. A scheme of the computed situations and energy differences is displayed in Figure 2. All the optimizations have been constrained to planarity within the C_{2v} symmetry; therefore, certain minima might represent an approximation to the fully relaxed geometries.

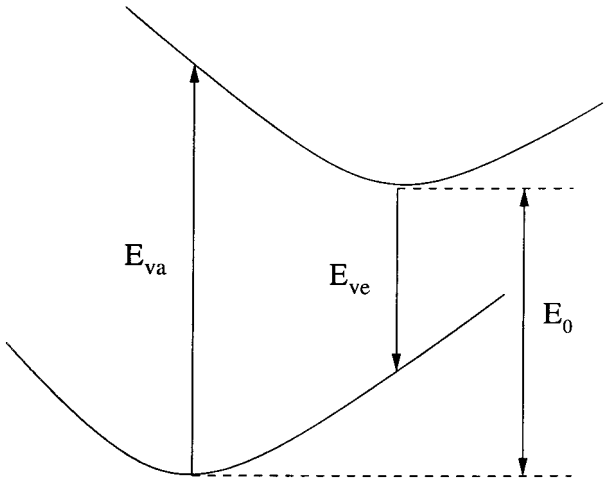

Figure 2. Scheme of the computed energy differences between two electronic states: E_{va}, vertical absorption; E_0, band origin; and E_{ve}, vertical emission.

The use of CASSCF geometries in this type of studies has been shown previously to be an adequate strategy to treat systems with delocalized bonds such as acridine.[43−49] Although no experimental geometry for acridine seems to be available, a recent CASSCF optimization of the geometry of a similar system such anthracene[50] gave bond distances within 0.01 Å from the experimental determinations. A similar accuracy can therefore be expected for acridine.

The main changes in the structure of the excited states with respect to the ground-state geometry occurs in the A_1 $\pi \rightarrow \pi^*$ (L_a) and B_1 $n \rightarrow \pi^*$ states, while the B_2 $\pi \rightarrow \pi^*$ (L_b) states keep the basic structure found in the optimal ground-state geometry. These trends related to the symmetry and character of the states can be found in many polyacene derivatives.[47] The $n \rightarrow \pi^*$ B_1 states, both singlet and triplet, are the product of an excitation from the in-plane σ nitrogen nonbonding lone pair to the out-of-plane π structure. The consequences of this transition in the geometry are important. In both states, the aromatic character increases in the benzenic rings: shortening of the single bonds and enlarging of the double bonds, while the C−N distance increases, a result of the loss of electronic density near the nitrogen atom to be shared with the terminal rings. The largest changes upon relaxation can be noted, however, in the geometry of the A_1 $\pi \rightarrow \pi^*$ (L_a) excited states, both singlet and triplet. A pronounced interchange in the bond alternation of the benzenic rings is expected to have a significant influence in the energy of the state and large vibrational progressions along the C−C stretching modes can be predicted. Finally, the geometrical changes in the B_2 $\pi \rightarrow \pi^*$(L_b) states are small, although a slight expansion of the molecule takes place, consistent with the results of vibrational spectroscopy, showing intense 0_0^0 transitions and short Franck−Condon progressions.[13,23] The behavior of the L_a and L_b states is similar to that found in the equivalent states of analogous compounds.[44,45,47]

3.2 Absorption Spectrum. The structure of excited states of acridine can be immediately related to that of anthracene, the equivalent fused ring polyacene. In anthracene,[50] configurations involving the three highest occupied and the three highest unoccupied π orbitals give rise, predominantly, to three pairs of excited states and excitations, the dipole-allowed B_{3u} and

TABLE 2: Composition of the PMCAS-CI Wave Function of the Low-lying Valence States of Acridine at the Ground State Geometry

state[a]	configuration[b]	label[c]	%[b]	Platt's state
1^1A_1 (ground state)	$(22a_1)^2(2b_1)^2(2a_2)^2$ $(3b_1)^2(3a_2)^2(4b_1)^2$		83	
1^1B_2 ($\pi\rightarrow\pi^*$)	$(3a_2)^1\rightarrow(5b_1)^1$	H-1→L	53	^1L_b
	$(4b_1)^1\rightarrow(4a_2)^1$	H→L+1	18	
2^1A_1 ($\pi\rightarrow\pi^*$)	$(4b_1)^1\rightarrow(5b_1)^1$	H→L	74	^1L_a
1^1B_1 ($n\rightarrow\pi^*$)	$(22a_1)^1\rightarrow(5b_1)^1$		81	
2^1B_2 ($\pi\rightarrow\pi^*$)	$(2a_2)^1\rightarrow(5b_1)^1$	H-2→L	45	
	$(4b_1)^1\rightarrow(4a_2)^1$	H→L+1	16	
3^1B_2 ($\pi\rightarrow\pi^*$)	$(2a_2)^1\rightarrow(5b_1)^1$	H-2→L	19	^1B_b
	$(3a_2)^1\rightarrow(5b_1)^1$	H-1→L	16	
	$(4b_1)^1\rightarrow(4a_2)^1$	H→L+1	31	
3^1A_1 ($\pi\rightarrow\pi^*$)	$(3a_2)^1\rightarrow(5a_2)^1$	H-1→L+2	12	
	$(4b_1, 4b_1)\rightarrow(5b_1, 5b_1)^2$	H,H→L,L	28	
4^1B_2 ($\pi\rightarrow\pi^*$)	$(4b_1)^1\rightarrow(5a_2)^1$	H→L+2	55	
1^1A_2 ($n\rightarrow\pi^*$)	$(22a_1)^1\rightarrow(4a_2)^1$		69	
4^1A_1 ($\pi\rightarrow\pi^*$)	$(4b_1)^1\rightarrow(6b_1)^1$	H→L+3	37	
5^1A_1 ($\pi\rightarrow\pi^*$)	$(3a_2)^1\rightarrow(5a_2)^1$	H-1→L+2	17	
	$(4b_1)^1\rightarrow(6b_1)^2$	H→L+3	11	
	$(4b_1, 4b_1)\rightarrow(5b_1, 5b_1)^2$	H,H→L,L	11	
6^1A_1 ($\pi\rightarrow\pi^*$)	$(3a_2)^1\rightarrow(4a_2)^1$	H-1→L+1	59	^1B_a
2^1B_1 ($\pi\rightarrow 3s$)	$(4b_1)^1\rightarrow(3s)^1$	H→3s	79	
5^1B_2 ($\pi\rightarrow\pi^*$)	$(3a_2)^1\rightarrow(6b_1)^1$	H-1→L+3	55	
7^1A_1 ($\pi\rightarrow\pi^*$)	$(3b_1)^1\rightarrow(5b_1)^1$	H-3→L	28	
	$(2b_1)^1\rightarrow(5b_1)^2$	H-4→L	11	
	$(4b_1)^1\rightarrow(7b_1)^2$	H→L+4	11	

[a] States labeled using the MS−CASPT2 order. [b] Configurations with weights (%) larger than 10%. [c] HOMO (H) and LUMO (L).

B_{2u} transitions, and the dipole-forbidden B_{1g} transitions. According to their basic configurational composition, the states can be classified following Platt's rules.[22] In particular, Platt's L and B states involve excitations between the two high-lying occupied orbitals (HOMO, HOMO-1) and the two low-lying unoccupied orbitals (LUMO, LUMO+1), hereafter HOMO (H) and LUMO (L). This classification is a useful way to discuss states and transitions that have similar behavior in polyacenes. The symmetric and antisymmetric combination of the excitations H → L+1 and H−1 → L (both one-electron promotions are close in energy) originates two B_{3u} states, labeled L_b and B_b (states or bands). The H → L and H−1 → L+1 configurations give rise to the B_{2u} states, labeled L_a and B_a, respectively. The inclusion of new orbitals into the description produces new states and transitions, such as the dipole-forbidden excitations to the B_{1g} states. By symmetry restrictions, only the transitions to the $^1B_{3u}$ and $^1B_{2u}$ states will lead to important bands in the absorption spectrum of anthracene. Excitations to the 1^1B_{3u} and 1^1B_{2u} states represent the ^1L_b (low intensity) and ^1L_a (medium) bands in Platt's nomenclature, respectively, while transitions to the 2^1B_{3u} and 3^1B_{2u} states constitute the ^1B_b (strong) and ^1B_a (medium) bands, respectively.[50] As in acridine there are no $\pi \rightarrow \pi^*$ dipole-forbidden transitions, the corresponding B_{1g} excitations in anthracene will become dipole allowed, but weak, transitions of the B_2 symmetry in acridine. Comparison of the transitions in anthracene with the values in acridine, compiled in Tables 2 and 3, reveals the similarity in the main bands of their spectra.

The absorption spectrum of acridine up to 6 eV has three different band systems.[19,20] Starting at 3.2 eV, a medium-intensity and highly structured band is displayed up to 4.1 eV, with prominent peaks that are almost invariant with the solvent. In ethanol, three main peaks are observed at 3.27, 3.50 (the most intense), and 3.66 eV.[2,19,20] Following, and beginning with a shoulder near 4.6 eV,[19,20] the most intense band of the spectrum peaks near 5.0 eV (4.98 eV in ethanol[19]) and continues with a long tail toward higher energies. The third feature is a broad band ranging from 5.8 to 6.0 eV measured in alcohols,[2,19,20] ethyl ether, and acetonitrile.[2]

TABLE 3: Vertical Excitation Energies (ΔE, eV), Oscillator Strengths (f), and State Dipole Moments (μ, D) in Acridine[a]

	theor					exptl	
state	ΔE_{PCAS} [b]	ΔE_{MPT2} [b]	f	μ	Platt's[b]	ΔE	f[c]
1^1A_1				1.97			
1^1B_2 ($\pi\rightarrow\pi^*$)	4.18	3.58	0.120	1.98	^1L_b	3.5[d]	0.09
2^1A_1 ($\pi\rightarrow\pi^*$)	5.20	3.77	0.101	3.45	^1L_a		
1^1B_1 ($n\rightarrow\pi^*$)	4.20	3.87	0.003	−0.31			
2^1B_2 ($\pi\rightarrow\pi^*$)	6.12	4.59	0.274	3.51		4.6[e]	
3^1B_2 ($\pi\rightarrow\pi^*$)	7.08	4.98	1.460	2.91	^1B_b	5.0[f]	1.0
3^1A_1 ($\pi\rightarrow\pi^*$)	6.02	5.02	0.009	2.41			
1^1A_2 ($n\rightarrow\pi^*$)	5.91	5.18	−	−0.35			
4^1B_2 ($\pi\rightarrow\pi^*$)	6.62	5.19	0.033	3.41			
4^1A_1 ($\pi\rightarrow\pi^*$)	6.58	5.36	0.008	1.35			
5^1A_1 ($\pi\rightarrow\pi^*$)	6.65	5.54	0.044	2.41			
6^1A_1 ($\pi\rightarrow\pi^*$)	7.58	5.69	0.118	2.18	^1B_a	5.6−5.7[e]	
2^1B_1 ($\pi\rightarrow 3s$)[i]	5.80	5.84	0.004	0.02			
5^1B_2 ($\pi\rightarrow\pi^*$)	6.89	5.93	0.132	0.61		5.9[f]	0.11
7^1A_1 ($\pi\rightarrow\pi^*$)	7.37	6.00	0.002	2.15			
1^3A_1 ($\pi\rightarrow\pi^*$)	2.83	2.48	−	2.56		2.2−2.3[g]	
1^3B_2 ($\pi\rightarrow\pi^*$)	3.96	3.32	−	1.78		3.4[h]	
1^3B_1 ($n\rightarrow\pi^*$)	4.29	3.59	−	−0.48			

[a] Experimental absorption maxima and theoretical, vertical results at the ground-state geometry. [b] PCAS: PMCAS-CI. MPT2: MS-CASPT2. Platt's: Platt's bands (see text). [c] From extinction coefficients in acetonitrile.[2] Normalized to unity for ^1B_b. [d] Spectra in different solvents.[2,7,10,11,19,20] [e] Shoulders in the low-energy side of the most intense bands.[20] [f] Most intense band (5.0 eV) and broad band (5.9 eV) measured in different solvents.[2,19,20] [g] High-pressure oxygen spectrum.[55] [h] Spectrum in neon matrices.[23] [i] The valence basis set was enlarged with an s Rydberg function (see text).

Table 3 lists the computed PMCAS-CI and MS-CASPT2 transition properties for acridine at the ground-state geometry, related to the vertical absorption (E_{va}). Analysis of the PMCAS-CI wave functions confirms the resemblance of the excited state structure in acridine and anthracene, even when the symmetry of the molecule has been lowered to C_{2v} in the former (see Table 2). Three low-lying states have been computed to lie vertically at the MS-CASPT2 level: 1^1B_2 at 3.58 eV (oscillator strength 0.120), 2^1A_1 at 3.77 eV (0.101), and 1^1B_1 at 3.87 eV (0.003). While the latter is an $n \rightarrow \pi^*$ state, the other two give rise to $\pi \rightarrow \pi^*$ transitions. As shown in Table 2, the transitions to the 1^1B_2 and 2^1A_1 states can be related to the ^1L_b and ^1L_a bands of Platt's model, respectively. The structured band found in the absorption spectra of acridine from 3.2 to 4.1 eV certainly contains the overlap of the three transitions. Figure 3 displays the highest occupied and lowest unoccupied molecular orbitals obtained at the SCF level. Some basic trends can be predicted on the basis of the orbital shapes and the composition of the wave functions. For instance, the 2^1A_1state, mainly described as H → L, is expected to relax its geometry via the interchange of the benzene ring bond alternation, as the topology of the H ($4b_1$) and L ($5b_1$) orbitals indicates. As regards the 1^1B_1 state, described as $n \rightarrow$ L, the charge transfer from the central σ system to the terminal π system and the final similarity of the benzene ring bonds can be also expected. The actual optimized geometries confirm such trends (see Table 1).

The vertical absorption energies (E_{va}), the computed band origins (E_0), and the vertical emission (E_{ve}) for the three low-lying singlet excited states are compiled in Table 4 (see also Figure 2), together with the available experimental data (experimental band origins, E_{00}). It can be clearly seen that the largest relaxation (0.7 eV) takes place for the 1^1B_1 $n \rightarrow \pi^*$ state, becoming the lowest adiabatically (S_1) for the isolated system.

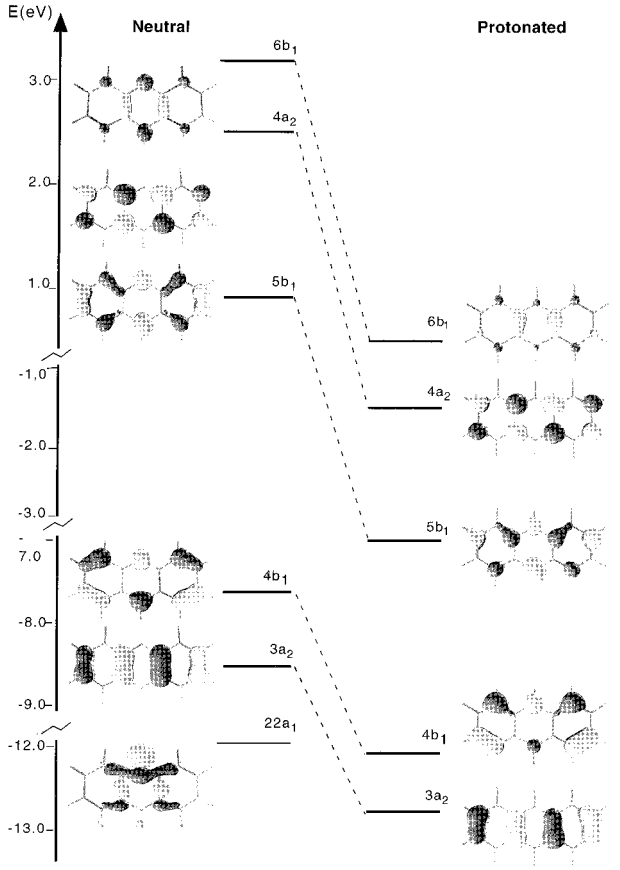

Figure 3. Highest occupied and lowest unoccupied molecular orbitals, labels, and energies computed at the SCF level for the acridine (Neutral) molecule and its acridinium (Protonated) ion.

TABLE 4: Calculated and Experimental Energy Differences (eV) for the Low-lying Excited Valence Singlet States of Acridine[a]

	theor			exptl		
states	E_{va}	E_0	E_{ve}	E_{va}	$E_{0_0^0}$	E_{ve}
1^1B_2 ($\pi\rightarrow\pi^*$) ^1L_b	3.58	3.28	3.28	3.5[b]	3.48[c]	
2^1A_1 ($\pi\rightarrow\pi^*$) ^1L_a	3.77	3.34	2.71		3.23[c]	2.88[d]
1^1B_1 ($n\rightarrow\pi^*$)	3.87	3.18	2.57		3.16[c]	3.0[e]

[a] E_{va}: Vertical absorption energy from the ground-state minimum. E_0: Computed band origin (see Figure 2). $E_{0_0^0}$: Experimental band origin. E_{ve}: Vertical emission energy from the excited-state minimum to the ground state. [b] Absorption maximum in different solvents.[2,7,10,11,19,20] [c] Suggested band origins in biphenyl crystal hosts.[13] [d] Fluorescence maximum in alkaline water.[7,11] [e] Fluorescence maximum in nonpolar solvents[6,7,10] (see text).

The other two states have similar relaxations (close to 0.4 eV), maintaining the same relative ordering. The main peaks observed in the lowest band at 3.27, 3.50, and 3.66 eV do not change their position on different solvents.[7,10−12,19−21] Considering the vibrationally structured character of the ^1L_b band in other related systems,[45] it is reasonable to assign these peaks to the vibrational progressions on the 1^1B_2 state. It has a computed dipole moment of magnitude similar to that of the ground state. The dipole moments for the 2^1A_1 (^1L_a) and 1^1B_1 states, 3.45 and −0.31 D, respectively, differ, however, from the ground-state value. Accordingly, red and blue shifts can be expected for the corresponding transitions in polar solvents. Zanker and Schmid[20] measured the polarization spectrum of acridine in ethanol. They reported a sudden change in the polarization of the low-lying band near 3.4 eV. Their interpretation of this experiment seems clear. The band origin corresponds in ethanol to the short-axis polarized ^1L_a (2^1A_1) state while the observed peaks at higher energies are related to the long-axis polarized ^1L_b (1^1B_2) state. The same order for the $\pi \rightarrow \pi^*$ states is proposed by Narva and McClure[13] in the spectrum of acridine in a biphenyl host crystal. The reverse ordering of the $\pi \rightarrow \pi^*$ states with respect to the present theoretical results might be related to the limit in the accuracy of the methodology (the energy difference is less than 0.1 eV), although we cannot compare to data measured in the vapor. It is expected that solvent effects (excimer effects in crystals) stabilize the 2^1A_1 state, with higher dipole moment, more than the 1^1B_2 state.

Aaron et al.[2] estimated ground and excited singlet-state dipole moments of acridine by the solvatochromic method. They concluded that in dioxane the dipole moment of S_1 is almost twice that of the ground state. The ratio between the dipole moments of S_0 and S_1 is consistent with the presence of the 2^1A_1 (^1L_a) state as the lowest adiabatic singlet excited state in polar environments. The red shift observed in the low-energy tail of the 3.2−4.1 eV absorption band of acridine upon increasing solvent polarity, for instance in the series hexane, acetonitrile, and ethanol,[6] is consistent with the ^1L_a state as the lowest in polar environments, a common situation in polyacene derivatives such as indoles[45,47,51] or purines.[52,53]

Calculations were made at the same CASSCF/MS-CASPT2 level on the protonated acridine molecule. The consequences on the two low-lying singlet excited states are within expectations. Figure 3 displays the stabilization experienced by the orbital energies of the protonated system, more pronounced for the virtual orbitals. As a result, on protonation, the transition to the 2^1A_1 ^1L_a state (H → L) decreases its energy by 0.42 eV and its oscillator strength by a half of the value in acridine. The transition to the 1^1B_2 ^1L_b state is within 0.1 eV with respect to its counterpart in acridine, and the oscillator strength decreases just slightly. The rest of the spectrum, except for the absence of the $n \rightarrow \pi^*$ transitions, remains basically unaltered. These results agree perfectly with the experiments. Ryan et al.[11] have reported spectra of acridine at different pH values. On increasing the acidity of the medium, a new broad shoulder has been detected in the low-energy tail of the absorption band of acridine, while the band maximum, corresponding to the 1^1B_2 transition, is unaltered.

The band system that has the strongest peak at 5.0 eV begins with a shoulder around 4.6 eV.[20] The computed spectrum places the transition to the 2^1B_2 state at 4.59 eV with an intermediate oscillator strength, 0.274. The state, having H−2 → L character, has a large dipole moment, 3.51 D. The excitation to the 3^1B_2 (^1B_b) state is computed at 4.98 eV with the largest oscillator strength value, 1.460. It can be easily related to the most intense feature of the spectrum measured near 5.0 eV in different solvents.[2,19,20] A number of transitions computed in the energy interval 5.0−5.4 eV are probably obscured in the recorded spectrum because of their overlap with the most intense band. Those are the transitions to the 3^1A_1 state at 5.02 eV, which has a pronounced doubly excited character, to the 1^1A_2 state at 5.18 eV (second $n \rightarrow \pi^*$ state), to the 4^1B_2 state at 5.19 eV, and to the 4^1A_1 state at 5.36 eV. Above 5.4 eV, the measured spectra of acridine have a broad band centered near 5.9 eV in different solvents.[2,19,20] The computed absorption spectrum of acridine predicts a number of transitions in that region. The 5^1A_1 excitation is placed at 5.54 eV with an oscillator strength of 0.044. The 6^1A_1 transition, corresponding to the ^1B_a Platt's band, is obtained at 5.69 eV with a nonnegligible oscillator strength, 0.118. Finally, the 5^1B_2 transition, H−1 → L+3 in nature, is computed at 5.93 eV with an oscillator strength of

0.132. The excitation to the 5^1B_2 state is probably responsible for the broad band at 5.9, while the long tail in the low-energy side near 5.5−5.6 eV in ethanol[20] can be better attributed to the transition to the 6^1A_1 (^1B_a) state. In relation to the ^1B_a state, mainly composed (59%) by the singly excited configuration H−1 → L+1, a large geometrical relaxation on the geometry optimization can be predicted considering the topology of the involved orbitals displayed in Figure 3, mainly because of the enlargement of the C−C bond lengths parallel to the short axis of the molecule. As regards the solvent effects on these bands, the high dipole moment of the 6^1A_1 state, 2.18 D, and the low dipole moment of the 5^1B_2 state, 0.61 D, lead to predict a red and a blue shift of the observed bands, respectively, in polar solvents.

Finally, we have also explicitly computed the transition to the lowest Rydberg state of the spectrum. The 2^1B_1 ($\pi \rightarrow 3s$) state of acridine is located at 5.84 eV. We consider this an upper limit for the proper calculation of the valence states skipping the inclusion of Rydberg functions. Above 6.0 eV, a full calculation including simultaneously valence and Rydberg functions would be necessary to get an accurate description of the states. This Rydberg series should converge to the first ionization potential of the molecule at 7.88 eV.[54]

The low-lying excitations in the singlet−triplet absorption spectrum of the acridine molecule have also been calculated. The $S_0 \rightarrow T_1$ absorption, involving the 1^3A_1 (H → L, ^3L_a) state, is found at 2.48 eV. Next, the 1^3B_2 (^3L_b) state at 3.32 eV is computed, while the third vertical state corresponds to the 1^3B_1 $n \rightarrow \pi^*$ at 3.59 eV. As it occurs for the singlet excited states, the relaxation of the $n \rightarrow \pi^*$ state is more pronounced and there is a change of order for the band origin of the 1^3B_1 and 1^3B_2 states in the isolated system. The 1^3A_1 state becomes the lowest in any case, and the large energy difference with respect to the 1^3B_1 $n \rightarrow \pi^*$ state, 1.11 eV, prevents any further change in the state ordering even in polar solvents. The computed vertical absorption energies for the $\pi \rightarrow \pi^*$ triplet states, 2.48 and 3.32 eV, respectively, are close to those computed at a comparable level of theory for the corresponding polyacene, anthracene: 2.00 and 3.40 eV, respectively.[50]

The measurements of the singlet−triplet spectrum of acridine have certain obscure points which should be clarified. The phosphorescence band origin from T_1 has been clearly established near 1.96 eV in ethanol[7,12] and neon matrices.[23] Evans[55] has reported a singlet−triplet absorption of acridine in high-pressure oxygen matrices starting at 1.96 eV, with maximum near 2.2−2.3 eV. All these data clearly match to the computed absorption band maximum (2.48 eV) and origin (1.75 eV) for the 1^3A_1 $\pi \rightarrow \pi^*$ T_1 state. From the comparison of the T_1 band origin and triplet−triplet absorption data, Kasama et al.[7] estimated the T_2 band origin near 3.2 eV in ethanol. This is also consistent with our computed 0_0^0 transition for the 1^3B_2 $\pi \rightarrow \pi^*$ state at 3.09 eV. Prochorow et al.[23] have reported a phosphorescence excitation spectrum of acridine in neon matrices, monitored to the $T_1 \rightarrow S_0$ band origin at 1.96 eV, and a band starting at 3.3 eV with a maximum near 3.4 eV. On the basis of our computed results, we can confirm that this absorption does not correspond to the $S_0 \rightarrow T_1$ transition, but to the $S_0 \rightarrow T_2$ $\pi \rightarrow \pi^*$ involving the 1^3B_2 state, with a band origin at 3.09 eV, an absorption maximum at 3.32 eV, and a predicted relaxed emission at 2.97 eV. Nevertheless, contributions to the observed band from the transition related to the 1^3B_1 $n \rightarrow \pi^*$ state cannot be ruled out.

3.3 Triplet−Triplet Absorption Spectrum. The triplet−triplet (T−T) absorption spectrum of acridine has been recorded in benzene, ethanol, and alkaline water.[7,12] The spectrum has been used to locate high triplet states of acridine and to understand the global photophysics of the system by studying the formation rate of T_1, which corresponds to the total radiationless decay rate of S_1.[8] The 1^3A_1 $\pi \rightarrow \pi^*$ state has been found to be the lowest triplet state at all levels of theory. Consequently, the low-lying T−T absorption spectrum was computed at this geometry. The T−T results are compiled in Table 6. The lowest excited state corresponds to the 1^3B_2 $\pi \rightarrow \pi^*$ state, computed at 1.49 eV with a related oscillator strength 0.017. The second transition involves the 1^3B_1 $n \rightarrow \pi^*$ state at 1.72 eV and has a low associated oscillator strength. The remaining spectrum up to 3.5 eV is composed of a number of $\pi \rightarrow \pi^*$ transitions, most of them weak, except for that to the 4^3B_2 state, computed at 2.94 eV with the largest oscillator strength, and the $1^3A_1 \rightarrow 5^3B_2$ transition at 3.46 eV with a moderate intensity.

The assignment of the measured T−T spectra is quite straightforward. Two band systems are observed. A very weak and structured feature is found from 1.26 to 1.98 eV, with its maximum at 1.26 eV. There is not full agreement in the literature about the influence of solvent effects on the band. Indeed, the available data are contradictory. While Kasama et al.[7] have reported a shift of 0.2 eV toward higher energies on changing the solvent from benzene to alkaline water, Periasamy[15] has informed that a small displacement to lower energies occurs from hexane and benzene to alkaline water. The present calculations give support to the finding of Periasamy.[15] The dipole moment of T_1 (1^3A_1) is computed to be somewhat smaller than that of T_2 (1^3B_2), both at the T_1 and T_2 optimized geometries. A small red shift in the lowest energy and of the

TABLE 5: Calculated and Experimental Energy Differences (eV) for the Low-lying Excited Valence Triplet States of Acridine with Respect to the Singlet Ground State[a]

	theor			exptl		
states	E_{va}	E_0	E_{ve}	E_{va}	$E_{0_0^0}$	E_{ve}
1^3A_1 ($\pi \rightarrow \pi^*$) ^3L_a	2.48	1.75	1.75	2.2−2.3[b]	1.96[b−d]	1.96[c,d]
1^3B_2 ($\pi \rightarrow \pi^*$) ^3L_b	3.32	3.09	2.97	3.4[d]	3.2−3.3[c,d]	
1^3B_1 ($n \rightarrow \pi^*$)	3.59	2.90	2.37			

[a] E_{va}: Vertical absorption energy from the ground-state minimum. E_0: Computed band origin (see Figure 2). $E_{0_0^0}$: Experimental band origin. E_{ve}: Vertical emission energy from the excited-state minimum to the ground state. [b] High-pressure oxygen spectrum.[55] [c] Spectrum in ethanol.[7,12] [d] Spectrum in neon matrices.[23]

TABLE 6: Vertical Excitation Energies (ΔE, eV), Oscillator Strengths (f), and State Dipole Moments (μ, D) for the Triplet States of Acridine at the 1^3A_1 State Optimized Geometry

	theor					exptl
state	ΔE_{PCAS} [a]	ΔE_{MPT2} [a]	f	μ	Platt's[a]	ΔE
1^3A_1 ($\pi \rightarrow \rho^*$)				1.33	^3L_a	
1^3B_2 ($\pi \rightarrow \rho^*$)	1.69	1.49	0.017	1.90	^3L_a	1.26[b]
1^3B_1 ($n \rightarrow \rho^*$)	1.52	1.72	0.001	−0.42		
2^3B_2 ($\pi \rightarrow \rho^*$)	2.61	1.97	0.000	1.90		
2^3A_1 ($\pi \rightarrow \rho^*$)	3.04	2.37	0.000	0.65		
3^3B_2 ($\pi \rightarrow \rho^*$)	3.64	2.68	0.001	2.25		
3^3A_1 ($\pi \rightarrow \rho^*$)	3.35	2.77	0.002	1.48	^3B_a	
4^3B_2 ($\pi \rightarrow \rho^*$)	4.13	2.94	0.168	2.89	^3B_b	2.95[c]
4^3A_1 ($\pi \rightarrow \rho^*$)	3.61	3.17	0.002	1.48		
5^3B_2 ($\pi \rightarrow \rho^*$)	3.99	3.46	0.032	0.66		

[a] PCAS: PMCAS-CI. MPT2: MS-CASPT2. Platt's: Platt's bands (see text). [b] Absorption maximum in nonpolar solvents. A red-shift < 0.05 eV observed from hexane to alkaline water.[12,15] [c] Absorption maximum in the vapor.[9] The band maximum has a small red shift in polar solvents: 2.88 eV in hexane and 2.79 eV in alkaline water.[15]

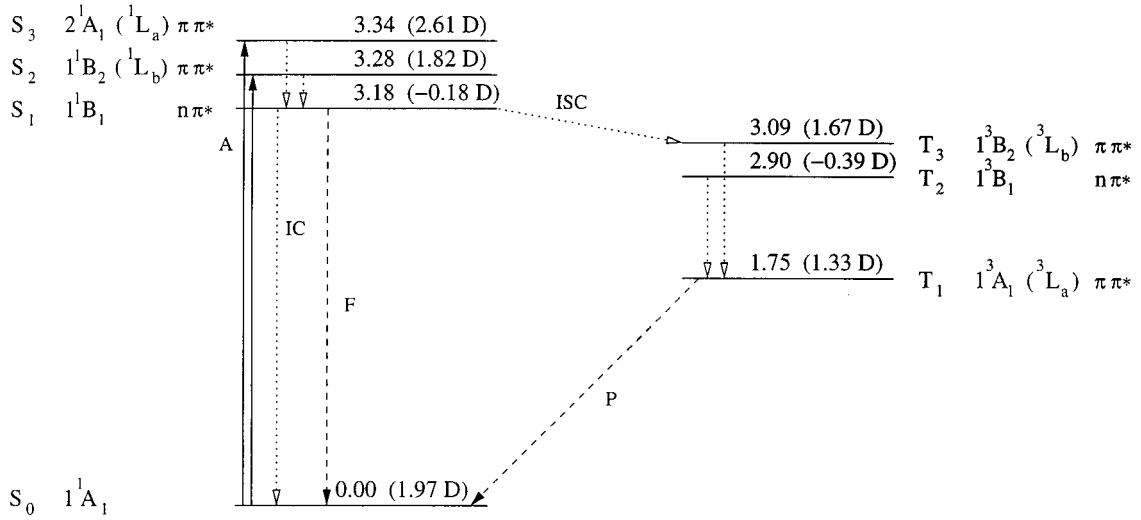

Figure 4. Scheme of the photophysics of acridine in the vapor based on the present computed results. Each state is represented with its relative band origin (in eV) and its corresponding dipole moment (in D, within parentheses) at its optimized geometry. The included processes are: A, absorption; ISC, intersystem crossing; IC, internal conversion; F, fluorescence, and P, phosphorescence.

T−T spectrum can be therefore expected as it was actually found by Periasamy.[15] It is also in agreement with another report of the band in ethanol peaking at 1.26 eV,[12] contradicting the measurement of Kasama et al.[7]

A second prominent and more intense peak is observed in the 2.8−2.9 eV region.[7,9,10,12,15] The experimental evidence clearly indicates in this case that the position of the band depends on the solvent polarity. The observed band maximum has been found at 2.95 eV in the gas phase.[9] It moves to 2.88 eV in hexane and 2.79 eV in alkaline water.[15] Our computed T−T spectrum has a transition with a large oscillator strength at 2.94 eV. It is the $1^3A_1 \rightarrow 4^3B_2$ vertical excitation of $\pi \rightarrow \pi^*$ character. The 4^3B_2 state has a dipole moment almost 1.5 D larger than that of the lowest triplet state, and therefore the observed red-shift is clearly understood. The report by Kasama et al.[7] showing no dependence of the energy of the band from benzene to water is probably wrong. In the region near 3.5 eV, the transition to the 5^3B_2 can be predicted to be observed in the T−T spectrum, although, to our knowledge, no experimental data are available at present.

3.4 Emission Spectra: Fluorescence and Phosphorescence. The emission spectra of acridine is strongly dependent on the properties of the environment. In the vapor, aprotic, nonhydrogen-bonding, and hydrocarbon solvents, acridine has virtually zero fluorescence quantum yields and fluorescence lifetimes in the picosecond range. In hydrogen-bonding solvents, i.e., alcohols and alkaline water, both the fluorescence quantum yields and lifetimes increase, the latter up to the nanosecond scale.[6,10,23] As in many N-heterocyclic and aromatic carbonyl compounds, the photophysics of acridine is controlled by the relative position of the close $n \rightarrow \pi^*$ and $\pi \rightarrow \pi^*$ low-lying singlet and triplet excited states of the molecule, a position that may be extremely perturbed by the solvent. Two models have been used to provide an explanation of the photophysics of acridine. First, a reversal of the two lowest singlet excited state has been suggested. While an $n \rightarrow \pi^*$ state could be the lowest S_1 state in the vapor and aprotic solvents, giving rise to a weak radiative process, a stabilized $\pi \rightarrow \pi^*$ state could become the S_1 state in polar and protic solvents, because of such environment destabilizes the $n \rightarrow \pi^*$ state, leading to an intense fluorescence (see, e.g., ref 23). A second model considers that it is the efficient vibronic coupling that occurs among close electronic states the responsible of the radiationless mechanisms that decreases the efficiency of the fluorescence process in nonpolar phases. The model is known, in general, as the proximity effect[24,25] and relies especially on the influence the solvent has on the state splitting. The solvent polarity would increase the state separation, decreasing the efficient $\pi \rightarrow \pi^*$ to $n \rightarrow \pi^*$ coupling and therefore decreasing the radiationless relaxation.[56,57] The consequence would be an intense emission from the $\pi \rightarrow \pi^*$ state in polar and protic solvents. In crystalline matrices of dimethylnaphthalene,[58] anthracene,[59,60] methyl methacrylate glasses,[7] and poly(vinyl alcohol) films,[61] the character of the S_1 state has been suggested to be $\pi \rightarrow \pi^*$, while in other matrices such as biphenyl, phenazine, and fluorene[13,62] an $n \rightarrow \pi^*$ is invoked as the lowest singlet excited state. An inherent stabilization of the $\pi \rightarrow \pi^*$ states by the arrangement of molecular dimers and the formation of excimers has been reported in acridine microcrystals.[10] As it has been proposed,[23] to consider the character of the lowest singlet state as $n \rightarrow \pi^*$ and $\pi \rightarrow \pi^*$ is just a zeroth-order description to describe a mixed situation dependent on the state separation, something which clearly changes under the solvent effects.

Figure 4 displays the energy-level diagram for the low-lying singlet and triplet states of isolated acridine computed at the MS-CASPT2 level. The excitation energies (eV) are band origins (E_0) and the dipole moments (D), obtained at the PMCAS-CI level, correspond to the states at their optimal geometry. It is believed that the present methodology yields accurately the relative position of the states, within 0.1−0.2 eV with respect to the actual data; further refinements are obviously out of the scope of the present study.

The 1^1B_1 $n \rightarrow \pi^*$ state is the lowest singlet excited state in isolated acridine. The geometrical relaxation from the vertical excitation at the ground-state geometry is large, near 0.7 eV, from 3.87 to 3.18 eV, as it is common in this type of transitions where the density charge moves from the σ to the π system.[46,47] The computed transition rate (Einstein's A_{21} coefficient) obtained using the transition dipole moment in absorption and the energy of the vertical emission (E_{ve}) toward the ground state, 2.57 eV (cf Table 4), is low, 8.12×10^4 s^{-1}, and the state has a large radiative lifetime of 12.3 μs. Consequently, in the vapor phase or nonpolar solvents, where the S_1 state has $n \rightarrow \pi^*$ character, the low intensity of fluorescence (proportional to A_{21}) can be predicted and the radiationless processes should prevail. It is necessary to bear in mind that the total emission rate of a

TABLE 7: Experimental and Computed Fluorescence Parameters in Acridine

Experimental[a]					
solvent	E_{max} (eV)	τ_F (ps)	ϕ_F	A_{21} (s^{-1})	τ_{rad} (ns)
vapor[c]	3.0	13	$<10^{-5}$	7.69×10^5	1300
hexane[d]	3.06	45	9.6×10^{-5}	2.13×10^6	470
benzene[d]	3.02	54	3.3×10^{-4}	6.13×10^6	163
ethanol[d]	2.99	350	7.9×10^{-3}	2.22×10^7	45
methanol[d]	2.97	377	0.0102	2.70×10^7	37
water[e]	2.88	11300	0.34	3.03×10^7	33

Theoretical[b]				
state	E_{max} (eV)	μ_{12} (au)	A_{21} (s^{-1})	τ_{rad} (ns)
1^1B_1	2.57	0.178	8.12×10^4	12300.0
2^1A_1	2.71	1.046	2.33×10^7	42.9
1^1B_2	3.28	1.170	5.18×10^7	19.3

[a] Selected experimental data. More values reported in refs 6, 8, 10. [b] μ_{12}: transition dipole moment in absorption. E_{max}: fluorescence maxima. See text for the other parameters. [c] Transient spectrum in the vapor.[9] [d] Time-resolved fluorescence in solution.[6] [e] Time-resolved fluorescence in alkaline water.[7]

transition ($1/\tau_F$) is related to the radiative ($1/\tau_{rad}$) and nonradiative ($1/\tau_{nonrad}$) rates by[41]

$$\frac{1}{\tau_F} = \frac{1}{\tau_{rad}} + \frac{1}{\tau_{nonrad}}$$

with τ_{rad} being large for transitions with a low transition dipole moment. Table 7 compiles the computed and measured data for the energy differences, lifetimes, and quantum yields related to the fluorescence process. The hypothesis of an S_1 $n \rightarrow \pi^*$ state seems confirmed by the data reported in the vapor,[9] hexane,[6,8] and benzene.[6,10] In all these environments the measured quantum yields (ϕ_F) and fluorescence lifetimes (τ_F) are low, $\approx 10^{-5}$ and $\approx 10^{-11}$ s, respectively. Considering that the relation between the radiative rate ($1/\tau_{rad}$) and the total decay rate ($1/\tau_F$) is the fluorescence quantum yield[41]

$$\phi_F = \tau_F/\tau_{rad}$$

the estimated radiative lifetime (τ_{rad}) in nonpolar solvents is about 10^{-6} s, clearly corresponding to a weak emission from the long-lived 1^1B_1 $n \rightarrow \pi^*$ state.

The 1^1B_2 $\pi \rightarrow \pi^*$ state is computed as the lowest singlet excited state in the vertical absorption spectrum. The geometrical relaxation decreases its energy with respect to the ground state by 0.3 eV. As can be seen in Table 1, the changes in the bond lengths and angles from the ground-state structure are small, as it is usual for the long-axis polarized ^1L_b states in other aromatic and heterocyclic compounds.[45] Transitions to these ^1L_b states usually produce structured bands where the origin transition corresponds to the most intense feature.[31] The band origin for the 1^1B_2 state is computed at 3.28 eV, as is the vertical emission. These results probably underestimate the Stokes shift, as previous experience indicates,[47,45] because the ^1L_b band origin is placed too low by the calculations. As it could be expected by its larger transition dipole moment, the computed fluorescence rate is much larger in the 1^1B_2 than in the 1^1B_1 state, and therefore the radiative lifetime falls in the region of nanoseconds: 19.3 ns. The 2^1A_1 $\pi \rightarrow \pi^*$ ^1L_a state relaxes 0.43 eV, yielding a band origin of 3.34 eV. The ^1L_a state optimized geometry is quite different from that of the ground state (see Table 1). For instance, the bond alternation in the rings reverses, as it occurred for the equivalent short-axis polarized ^1L_a states in many other systems.[44,45,47] The vertical emission (fluorescence maximum) is computed at 2.71 eV for this state, which represents a Stokes shift of 1.0 eV. The fluorescence rate for the 2^1A_1 state is computed to be 2.33×10^7 s^{-1} and its radiative lifetime, 42.9 ns, more than twice the calculated rate for the 1^1B_2 state.

As it was stated above, the experimental evidence in absorption points out the following order for the band origins of the transitions: 1^1B_1, 3.16 eV; 2^1A_1, 3.23 eV; and 1^1B_2, 3.48 eV. These assignments have been performed for acridine in a biphenyl crystal[13] and might be representative of the state ordering in nonpolar environments, although small excimer effects have to be considered in the matrix.[23] Compared to the theoretical results: 1^1B_1, 3.18 eV; 2^1A_1, 3.34 eV; and 1^1B_2, 3.28 eV there is a reversal in the order of the $\pi \rightarrow \pi^*$ states. One possibility is that the methodology employed is not accurate enough to give the appropriate ordering. In a nonpolar solvent such as benzene,[7,10] acridine has a weak and structured fluorescence band with maximum at 3.02 eV. In alkaline water[6,7,11,28] the band is broader and shifts slightly toward lower energies (maximum 2.88 eV). Considering the computed dipole moments of the states at their equilibrium geometries: 1^1B_1, -0.18 D; 1^1B_2, 1.82 D; and 2^1A_1, 2.61 D, compared to the ground-state value, 1.97 D, it is reasonable to expect a destabilization of the 1^1B_1 $n \rightarrow \pi^*$ state and a stabilization of the 2^1A_1 $\pi \rightarrow \pi^*$ state on increasing the interaction with the solvent. In the extremes of the scale we will find a low-lying $n \rightarrow \pi^*$ state in vapor giving rise to a nonfluorescent system ($\phi_F < 10^{-5}$, $\tau_F = 13$ ps[8,9]), while in alkaline water (to prevent protonation) the 2^1A_1 state will be stabilized to give a strong fluorescence ($\phi_F = 0.34$, $\tau_F = 33$ ns[7]) corresponding to the emission computed for the $\pi \rightarrow \pi^*$ states. In particular the 2^1A_1 state, with a computed $\tau_{rad} = 42.9$ ns, should get stabilized more than the 1^1B_2 state by the effect of polar solvents because of its larger dipole moment. Between the two situations, the vapor and aqueous phases, a crossing of the three states has probably taken place depending on the environment. One can suggest that there is no contradiction between the two models mentioned before to explain the acridine photophysics. The present results support the idea of a state reversal, from $n \rightarrow \pi^*$ to $\pi \rightarrow \pi^*$, for the lowest singlet state on increasing the solvent polarity, but obviously all states are close enough to make the vibronic interactions to play an important role in many of the environments. The absence of out-of-plane C−H bending modes neighbors to the nitrogen atom in acridine has been used, however, as an argument to diminish the importance of the vibronic coupling in this case.[24]

The dependence of the fluorescence maximum of acridine in different solvents was reported by Diverdi and Topp[6] to vary from 3.06 eV in hexane to 2.88 eV in alkaline water. The results in polar solvents agree with the computed fluorescence maximum for the 2^1A_1 ^1L_a state at 2.71 eV. The shift of the peak to higher energies for nonpolar environments, where the 1^1B_1 state is suggested to be the lowest singlet excited state, cannot be easily related and explained by the computed vertical emission from the 1^1B_1 minimum at 2.57 eV, lower than for the previous state. It must be pointed out, however, that the $n \rightarrow \pi^*$ state has a large geometry relaxation and, therefore, a large vibrational progression can be expected. This makes the usual assumption based on the Franck−Condon principle that relates vertical emission with emission band maximum to be probably less valid. Instead, the band maximum tends to the band origin around 3.2 eV.

The relative position of the triplet states is also of crucial importance when considering the photophysics of acridine. The

computed results displayed in Figure 4 place as the lowest triplet state the 1^3A_1 $\pi \rightarrow \pi^*$ ^1L_a state with a band origin of 1.75 eV and a dipole moment slightly smaller than that of the ground state. This state will keep the relative order despite any solvent effect due to the large energy separation with respect to the other electronic states. The relaxation from the vertical absorption is large, near 0.7 eV. Band origin and vertical emission are, however, computed at the same energy. Correspondingly, phosphorescent emission (band origin and maximum) has been measured at 1.96 eV in neon matrices[23] and ethanol.[7] The second triplet state is computed to be the 1^3B_1 $n \rightarrow \pi^*$ state, placed at 2.90 eV with a very small dipole moment, −0.39 D. This state will be destabilized in the presence of polar solvents, decreasing the separation with respect to the $\pi \rightarrow \pi^*$ singlet excited states, in particular to the ^1L_a state. Finally, the calculations in the isolated system place the T_3 1^3B_1 $\pi \rightarrow \pi^*(^1L_b)$ state at 3.09 eV with a dipole moment of 1.67 D, similar to that of the ground state, 1.97 D. It is known, experimentally, that the position of this state is almost solvent-independent.[15,58]

Considering the computed state ordering, the photophysics of acridine can be summarized as follows. In the vapor, the lowest $\pi \rightarrow \pi^*$ S_2 state is produced by optical excitation (S_3 $\pi \rightarrow \pi^*$ in a minor extent). Subsequently, a rapid internal conversion to the S_1 $n \rightarrow \pi^*$ state, close by near 0.1 eV, takes place. As the radiative lifetime of the $n \rightarrow \pi^*$ is large (in the order of microseconds), the nonradiative processes, intersystem crossing (ISC), and internal conversion (IC) will prevail, preventing the fluorescence to occur. An efficient intersystem crossing, S_1 ($n \rightarrow \pi^*$) to T_3 ($\pi \rightarrow \pi^*$), takes place (the computed energy separation is less than 0.1 eV) followed by internal conversion to the T_1 ($\pi \rightarrow \pi^*$) state. The internal conversion from S_1 to S_0 becomes also a very efficient process. Finally, a weak phosphorescence will be observed from T_1. Figure 4 includes the state ordering and properties, describing the overall mechanism schematically.

The relative position of the states will be perturbed by different effects, such as polarity of the environment,[6,7] excimer effects in crystal matrices,[13,23] temperature,[7,12] and acidity of the medium.[11] Focusing on the solvent effects and considering the energy and dipole moment values listed in Figure 4, the major perturbations upon increasing the solvent polarity are expected to occur for the 1^1B_1 (S_1) and 1^3B_1 (T_2) $n \rightarrow \pi^*$ states, and by the 2^1A_1 (S_3) $\pi \rightarrow \pi^*$ state, because of their small and large dipole moments, respectively. The $n \rightarrow \pi^*$ states experience a more pronounced destabilization, probably placing them above the $\pi \rightarrow \pi^*$ states. The 2^1A_1 state, on the contrary, and as it has been already discussed, will become the S_1 state on polar solvents such as ethanol or water. The photophysics of the system will be perturbed accordingly. To have an S_1 $\pi \rightarrow \pi^*$ state means to have an emission with short radiative lifetime (computed 42.9 ns for the 2^1A_1 state) leading to an intense fluorescence. In nonpolar solvents, an efficient ISC, S_1 ($n \rightarrow \pi^*$) → T_3 ($\pi \rightarrow \pi^*$), may occur,[56] enhancing the radiationless decay rate. The interchange of the singlet states to give an S_1 $\pi \rightarrow \pi^*$ state deactivates this type of relaxation path because of the unfavorable spin−orbit coupling between $\pi \rightarrow \pi^*$ states (new S_1 and T_3).[56] Another coupling may take place between the S_1 $\pi \rightarrow \pi^*$ and T_2 $n \rightarrow \pi^*$ states depending on their relative position and separation upon solvation. In the isolated system, the computed energy difference between the 2^1A_1 state (better candidate to become S_1 in polar solvents) and the 1^3B_1 state is 0.44 eV. The energy separation is too large to originate an effective coupling. It is more probable that an efficient ISC is produced with an increase in the temperature, and after the internal promotion from S_1 $\pi \rightarrow \pi^*$ to S_2 (or S_3) $n \rightarrow \pi^*$ followed by ISC toward T_3 $\pi \rightarrow \pi^*$, as it has been suggested[10] to explain the increase of ISC with temperature in polar solvents. Assuming the radiative rate constant to be temperature independent,[11] the decrease of τ_F with temperature reflects the dependence of τ_{nonrad}, that is, the nonradiative paths such as ISC. Other explanation could be related with the decrease of the $\pi \rightarrow \pi^*$−$n \rightarrow \pi^*$ energy gap by thermal activation (for instance by breaking hydrogen bonds), favoring the internal conversion to the S_0 state and decreases the fluorescence lifetime and intensity.[11]

The acridine photophysics has many other aspects that have been studied and discussed, such as the changes on the emission properties by protonation. The absence of $n \rightarrow \pi^*$ states and the presence of 2^1A_1 ^1L_a as the lowest singlet excited state upon protonation guarantees the intense fluorescence of the acridinium ion, recorded at pH 2 with a fluorescence maximum 0.3 eV lower than acridine in alkaline aqueous solutions.[11] Further effects such as those related to the dimerization of acridine,[26] the photophysics in solid matrices,[10] or photoreduction[12] can be found in the literature. To get insight into certain questions related to the acridine spectroscopy, we have, however, focused the present study to the characterization of the low-lying excited states of the isolated system, mainly because we are confident of the quantitative, predictive character of our theoretical results on electronic states. Studies are in their way on acridine derivatives with the aim to give an overall picture of the photophysics of this family of compounds.

4. Summary and Conclusions

Ab initio CASSCF and MS-CASPT2 calculations have been performed on the singlet and triplet $\pi \rightarrow \pi^*$ and $n \rightarrow \pi^*$ valence excited states of acridine. The geometries of the ground and low-lying singlet and triplet states have been optimized in order to obtain appropriate energy differences to study the spectroscopy of the system. Vertical absorption energies from the ground-state geometry, triplet−triplet absorption energies at the optimized geometry of the lowest triplet state, band origins between state relaxed minima, and vertical emissions from the relaxed minima of the excited states to the ground state have been computed together with other properties such as dipole moments and transition properties (oscillator strengths, radiative rates, and lifetimes). The lowest Rydberg state has also been located in the spectrum of acridine. In addition, calculations on the states of the acridinium ion have been performed in order to analyze the effects of protonation on the spectroscopy of the system.

The three main band systems observed in the spectrum of acridine in different solvents[2,19,20] have been fully assigned here. The lowest energy band of medium intensity reported from 3.2 to 4.1 eV has been found to be composed of three electronic transitions: $1^1A_1 \rightarrow 1^1B_2$ (^1L_b) and $1^1A_1 \rightarrow 2^1A_1$ (^1L_a), both $\pi \rightarrow \pi^*$ promotions computed vertically at 3.58 and 3.77 eV, respectively, and the $1^1A_1 \rightarrow 1^1B_1$ $n \rightarrow \pi^*$ transition computed to lie vertically at 3.87 eV. The latter becomes the lowest singlet excited state by geometry relaxation and has a band origin of 3.18 eV. The ^1L_b state at 3.28 eV is computed to be the second excited-state adiabatically, very close to the ^1L_a state at 3.34 eV. In polar solvents, and mainly because of the small (1^1B_1) and large (^1L_a) dipole moments of the states, the reverse ordering can be predicted, making the $\pi \rightarrow \pi^*$ ^1L_a state the lowest singlet excited state. This fact is consistent with the observed red shift in polar solvents and the dramatic change in the fluorescence quantum yield. In absorption, the band peaking at 5.0 eV is

mainly attributed to the transition to the 3^1B_2 ^1B_b state, while the broad band observed at 5.9 eV can be assigned to the excitation to the 5^1B_2 state. Shoulders to some of these bands have been also assigned to excitations of different states of the absorption spectrum. The lowest Rydberg transition has been located at 5.84 eV. Regarding the triplet−triplet spectrum, the two observed peaks at 1.26 and 2.95 eV have been assigned to the transitions to the second (1^3B_2) and eighth (4^3B_2) triplet states, and the contradictory dependence of these bands with the solvent found in the literature has been clarified. Finally, calculations on the low-lying states of the acridinium ion have established the stabilization of the 2^1A_1 ^1L_a state with respect to the analogous state of the neutral system, while the remaining states basically maintain their position and nature.

As regards the emission properties of acridine, the present findings support the model of a state reversal in the ordering of the low-lying singlet states upon increasing the polarity of the solvent. A scheme for the photophysics of acridine in the vapor has been built, where the $n \rightarrow \pi^*$ state is the S_1 nonfluorescent state and the radiationless processes are proposed as the main relaxation mechanisms on the basis of the relative position of the low-lying singlet and triplet states. The intense fluorescence of acridine in polar media can be easily rationalized by the expected energetic stabilization of the ^1L_a $\pi \rightarrow \pi^*$ state, predicted in terms of the computed dipole moment. In this manner, the ^1L_a $\pi \rightarrow \pi^*$ state becomes the short-lived, fluorescent S_1 state in polar solvents.

Acknowledgment. The research reported in this communication has been supported by the DGES project PB97-1377 of Spain, by the European Commission through the TMR network contract ERB FMRX-CT96-0079 (Quantum Chemistry for the Excited State), and by the Generalitat Valenciana. The authors would like to thank Dr. R. Pou-Amérigo for fruitful discussions.

References and Notes

(1) Fischer, G.; Pindur, U. *Pharmazie* **1999**, *54*, 83.
(2) Aaron, J. J.; Maafi, M.; Párkányi, C.; Boniface, C. *Spectrochim. Acta* **1995**, *A51*, 603.
(3) Acheson, R. M. *Heteroatomic cyclic compounds*; Wiley Interscience: New York, 1973.
(4) Adamczyk, M.; Fishpaugh, J. R.; Gleber, J. C.; Mattingly, P. G.; Shreder, K. *Eur. Mass. Spectrom.* **1998**, *4*, 121.
(5) Maskiewicz, R.; Sogah, D.; Bruice, T. C. *J. Am. Chem. Soc.* **1979**, *101*, 5347.
(6) Diverdi, L. A.; Topp, M. R. *J. Phys. Chem.* **1984**, *88*, 3447.
(7) Kasama, K.; Kikuchi, K.; Yamamoto, S. A.; Uji-Ie, K.; Nishida, Y.; Kokubun, H. *J. Phys. Chem.* **1981**, *85*, 1291.
(8) Sundstrom, V.; Rentzepis, P. M.; Lim, E. C. *J. Chem. Phys.* **1977**, *66*, 4287.
(9) Hirata, Y.; Tanaka, I. *Chem. Phys.* **1977**, *25*, 381.
(10) Asahi, T.; Furube, A.; Masuhara, H. *Bull. Chem. Soc. Jpn.* **1998**, *71*, 1277.
(11) Ryan, E. T.; Xiang, T.; Johnston, K. P.; Fox, M. A. *J. Phys. Chem. A* **1997**, *101*, 1827.
(12) Kikuchi, K.; Kasama, K.; Kanemoto, A.; Uji-Ie, K.; Kokubun, H. *J. Phys. Chem.* **1985**, *89*, 868.
(13) Narva, D. L.; McClure, D. S. *Chem. Phys.* **1981**, *56*, 167.
(14) Noe, L. J.; Degenkolb, E. O.; Rentzepis, P. M. *J. Chem. Phys.* **1978**, *68*, 4435.
(15) Periasamy, N. *Chem. Phys. Lett.* **1983**, *99*, 322.
(16) Goodman, L.; Harrell, R. W. *J. Chem. Phys.* **1959**, *30*, 1131.
(17) Wagner, R. W.; Hochmann, P.; El-Bayoumi, M. A. *J. Mol. Struct.* **1975**, *54*, 167.
(18) Rak, J.; Blaźejowski, J. *J. Photochem. Photobiol. A: Chem.* **1992**, *67*, 287.
(19) Perkampus, H. H. *UV-Vis Atlas of Organic Compounds*; VCH: Weinheim, 1992.
(20) Zanker, V.; Schmid, W. *Chem. Ber.* **1957**, *90*, 2253.
(21) Kasama, K.; Kikuchi, K.; Uji-Ie, K.; Yamamoto, S. A.; Kokubun, H. *J. Phys. Chem.* **1982**, *86*, 33.
(22) Platt, J. R. *J. Chem. Phys.* **1949**, *17*, 489.
(23) Prochorow, J.; Kozankiewicz, B.; Gemi, B. B. D.; Morawski, O. *Acta Phys. Pol., A* **1998**, *94*, 749.
(24) Lim, E. C. In *Excited States*; Lim, E. C., Ed.; Academic Press: New York, 1977; vol. 3.
(25) Wassam, W. A., Jr. In *Excited States*; Lim, E. C., Ed.; Academic Press: New York, 1982; vol. 5.
(26) Prochorow, J.; Deperasińska, I.; Morawski, O. *Chem. Phys. Lett.* **2000**, *316*, 24.
(27) Kasama, K.; Kikuchi, K.; Nishida, Y.; Kokubun, H. *J. Phys. Chem.* **1981**, *85*, 4148.
(28) Gafni, A.; Brand, L. *Chem. Phys. Lett.* **1978**, *58*, 346.
(29) Andersson, K.; Malmqvist, P.-Å.; Roos, B. O. *J. Chem. Phys.* **1992**, *96*, 1218.
(30) Finley, J.; Malmqvist, P.-Å.; Roos, B. O.; Serrano-Andrés, L. *Chem. Phys. Lett.* **1998**, *288*, 299.
(31) Roos, B. O.; Andersson, K.; Fülscher, M. P.; Malmqvist, P.-Å.; Serrano-Andrés, L.; Pierloot, K.; Merchán, M. In *Advances in Chemical Physics: New Methods in Computational Quantum Mechanics*; Prigogine, I., Rice, S. A., Eds.; John Wiley & Sons: New York, 1996, Vol. XCIII, p 219.
(32) Merchán, M.; Serrano-Andrés, L.; Fülscher, M. P.; Roos, B. O. In *Recent Advances in Multireference Theory*; Hirao, K., Ed.; World Scientific: Singapore, 1999; Vol. IV, p 161.
(33) Serrano-Andrés, L.; Roos, B. O. *Chem.−Eur. J. A* **1997**, *3*, 717.
(34) Molina, V.; Merchán, M.; Roos, B. O. *J. Phys. Chem. A* **1997**, *101*, 3478.
(35) Widmark, P.-O.; Malmqvist, P.-Å.; Roos, B. O. *Theor. Chim. Acta* **1990**, *77*, 291.
(36) Roos, B. O.; Fülscher, M. P.; Malmqvist, P.-Å.; Merchán, M.; Serrano-Andrés, L. In *Quantum Mechanical Electronic Structure Calculations with Chemical Accuracy*; Langhoff, S. R., Ed.; Kluwer Academic Publishers: Dordrecht, 1995; p 357.
(37) Andersson, K.; Malmqvist, P.-Å.; Roos, B. O.; Sadlej, A. J.; Wolinski, K. *J. Phys. Chem.* **1990**, *94*, 5483.
(38) Roos, B. O.; Andersson, K.; Fülscher, M. P.; Serrano-Andrés, L.; Pierloot, K.; Merchán, M.; Molina, V. *J. Mol. Struct. (THEOCHEM)* **1996**, *388*, 257.
(39) Malmqvist, P.-Å. *Int. J. Quantum Chem.* **1986**, *30*, 479.
(40) Malmqvist, P. Å.; Roos, B. O. *Chem. Phys. Lett.* **1989**, *155*, 189.
(41) McHale, J. L. *Molecular Spectroscopy*; Prentice Hall: New Jersey, 1999.
(42) Andersson, K.; Baryz, M.; Bernhardsson, A.; Blomberg, M. R. A.; Boussard, P.; Cooper, D. L.; Fleig, T.; Fülscher, M. P.; Hess, B.; Karlström, G.; Lindh, R.; Malmqvist, P.; Neogrady, P.; Olsen, J.; Roos, B. O.; Sadlej, A. J.; Schimmelpfennig, B.; Schütz, M.; Seijo, L.; Serrano, L.; Siegbahn, P. E.; Stålring, J.; Thorsteinsson, T.; Veryazov, V.; Wahlgren, U.; Widmark, P. *MOLCAS Version 5.0*., Department of Theor. Chem., Chem. Center, University of Lund, P.O. Box 124, S-221 00 Lund, Sweden, Lund, 2000.
(43) Serrano-Andrés, L.; Merchán, M.; Nebot-Gil, I.; Lindh, R.; Roos, B. O. *J. Chem. Phys.* **1993**, *98*, 3151.
(44) Serrano-Andrés, L.; Lindh, R.; Roos, B. O.; Merchán, M. *J. Phys. Chem.* **1993**, *97*, 9360.
(45) Serrano-Andrés, L.; Roos, B. O. *J. Am. Chem. Soc.* **1996**, *118*, 185.
(46) González-Luque, R.; Merchán, M. *Mol. Phys.* **1998**, *94*, 189.
(47) Serrano-Andrés, L.; Borin, A. C. *Chem. Phys.* **2000**, *262*, 267.
(48) Molina, V.; Merchán, M.; Roos, B. O.; Malmqvist, P.-Å. *Phys. Chem. Chem. Phys.* **2000**, *2*, 2211.
(49) Page, C. S.; Merchán, M.; Serrano-Andrés, L.; Olivucci, M. *J. Phys. Chem. A* **1999**, *103*, 9864.
(50) Kawashima, Y.; Hashimoto, T.; Nakano, H.; Hirao, K. *Theor. Chem. Acc.* **1999**, *102*, 49.
(51) Borin, A. C.; Serrano-Andrés, L. *J. Mol. Struct. (THEOCHEM)* **1999**, *464*, 121.
(52) Fülscher, M. P.; Serrano-Andrés, L.; Roos, B. O. *J. Am. Chem. Soc.* **1997**, *119*, 6168.
(53) Borin, A.; Serrano-Andrés, L.; Fülscher, M. P.; Roos, B. O. *J. Phys. Chem. A* **1999**, *103*, 1838.
(54) Hush, N. S.; Cheung, A. S.; Hilton, P. R. *J. Electron Spectrosc. Relat. Phenom.* **1975**, *7*, 385.
(55) Evans, D. F. *J. Chem. Soc.* **1957**, *257*, 1351.
(56) El-Sayed, M. A. *J. Chem. Phys.* **1963**, *38*, 2834.
(57) Shimakura, N.; Fujimura, Y.; Nakajima, T. *Chem. Phys.* **1977**, *19*, 155.
(58) Morawski, O.; Prochorow, J. *Acta Phys. Pol., A* **1995**, *88*, 469.
(59) Williams, J. O.; Clarke, B. P. *J. Chem. Soc., Faraday Trans. 2* **1977**, *90*, 2253.
(60) Morawski, O.; Kozankiewicz, B.; Prochorow, J.; Radomski, R. *Chem. Phys. Lett.* **1988**, *150*, 307.
(61) Kikuchi, K.; Uji-Ie, K.; Miyashita, Y.; Kokubun, H. *Bull. Chem. Soc. Jpn.* **1977**, *50*, 879.
(62) Prass, B.; Fujara, F.; Seiff, F.; Stehlik, D. *J. Lumin.* **1981**, *24*, 483.